Microwave spectrum, largeamplitude motions, and ab initio calculations for N2O5

J.U. Grabow, A. M. Andrews, G. T. Fraser, K. K. Irikura, R. D. Suenram, F. J. Lovas, W. J. Lafferty, and J. L. Domenech

Citation: The Journal of Chemical Physics **105**, 7249 (1996); doi: 10.1063/1.472586
View online: http://dx.doi.org/10.1063/1.472586
View Table of Contents: http://scitation.aip.org/content/aip/journal/jcp/105/17?ver=pdfcov
Published by the AIP Publishing

Microwave spectrum, large-amplitude motions, and *ab initio* calculations for N_2O_5

J.-U. Grabow,[a),b),c)] A. M. Andrews,[a),d)] G. T. Fraser,[a)]
K. K. Irikura,[e)] R. D. Suenram,[a)] F. J. Lovas,[a)] and
W. J. Lafferty[a)]
National Institute of Standards and Technology, Gaithersburg, Maryland 20899

J. L. Domenech
Instituto de Estructura de la Materia, CSIC, Serano 119, 28006 Madrid, Spain

(Received 21 March 1996; accepted 22 July 1996)

The rotational spectrum of dinitrogen pentoxide (N_2O_5) has been investigated between 8 to 25 GHz at a rotational temperature of ~2.5 K using a pulsed-molecular-beam Fourier-transform microwave spectrometer. Two weak *b*-dipole spectra are observed for two internal-rotor states of the molecule, with each spectrum poorly characterized by an asymmetric-rotor Hamiltonian. The observation of only *b*-type transitions is consistent with the earlier electron-diffraction results of McClelland *et al.* [J. Am. Chem. Soc. **105**, 3789 (1983)] which give a C_2 symmetry molecule with the *b* inertial axis coincident with the C_2 axis. Analysis of the ^{14}N nuclear hyperfine structure demonstrates that the two nitrogen nuclei occupy either structurally equivalent positions or are interchanging inequivalent structural positions via tunneling or internal rotation at a rate larger than ~1 MHz. For the two internal rotor states, rotational levels with K_a+K_c even have $I_N=0$, 2, while levels with K_a+K_c odd have $I_N=1$, where I_N is the resultant nitrogen nuclear spin. This observation establishes that the equilibrium configuration of the molecule has a twofold axis of symmetry. Guided by *ab initio* and dynamical calculations which show a planar configuration is energetically unfavorable, we assign the spectrum to the symmetric and antisymmetric tunneling states of a C_2 symmetry N_2O_5 with internal rotation tunneling of the two NO_2 groups via a geared rotation about their respective C_2 axes. Because of the Bose–Einstein statistics of the spin-zero oxygen nuclei, which require that the rotational–vibrational–tunneling wave functions be symmetric for interchange of the O nuclei, only four of the ten vibrational-rotational-tunneling states of the molecule have nonzero statistical weights. Model dynamical calculations suggest that the internal-rotation potential is significantly more isotropic than implied by the electron-diffraction analysis. © *1996 American Institute of Physics.* [S0021-9606(96)02740-7]

I. INTRODUCTION

The highly reactive dinitrogen pentoxide (N_2O_5) molecule plays an important role in the chemistry of the upper atmosphere, functioning as a nighttime reservoir for NO_2 and NO_3, both of which are implicated in the catalytic destruction of stratospheric ozone. Direct evidence for the presence of N_2O_5 in the stratosphere has been obtained by Toon *et al.*[1] from infrared spectra recorded at sunrise by the Atmospheric Trace Molecule Experiment aboard Spacelab 3. Their results have generated renewed interest in the spectroscopy of N_2O_5, motivating efforts[2–6] to measure precise spectroscopic parameters for modeling the band profiles used in extracting the atmospheric concentration of N_2O_5. Despite all this effort, no rotationally resolved infrared spectrum has been reported for this species, which could provide the necessary spectroscopic constants for simulating the atmospheric spectrum as a function of temperature.

A starting point in any high-resolution spectroscopic study of N_2O_5 is the electron-diffraction results of McClelland *et al.*[7] Their experiments show that N_2O_5 has a nonplanar geometry with two equivalent NO_2 groups joined by an oxygen atom to form a C_2 symmetry configuration with a strongly bent $O_2N–O–NO_2$ angle of 111.8(6)° (see Fig. 1). To adequately model the electron-diffraction patterns, McClelland *et al.*[7] invoked large-amplitude torsions of the NO_2 groups about their C_2 axes. They modeled the torsional potential using atom–atom Lennard-Jones repulsions between the oxygen atoms on opposing NO_2 groups, supplemented by cosine potentials in the internal rotation angles to mimic any electronic effects propagated through the N–O–N backbone.

The structural results of McClelland *et al.*[7] are qualitatively supported by Hartree–Fock calculations using small 4–31 G basis sets[8] and by density-functional calculations using Gaussian-type orbitals and triple-zeta-plus-polarization basis sets.[9] The more recent density-functional calculations[9]

[a)]Optical Technology Division.
[b)]NIST Guest Researcher.
[c)]Present address: Institut für Physikalische Chemie, Christian-Albrechts-Universität, D-24098 Kiel, Germany.
[d)]Permanent address: Science and Technology Division, Institute for Defense Analysis, 1801 N. Beauregard Street, Alexandria, VA 22311.
[e)]Physical and Chemical Properties Division.

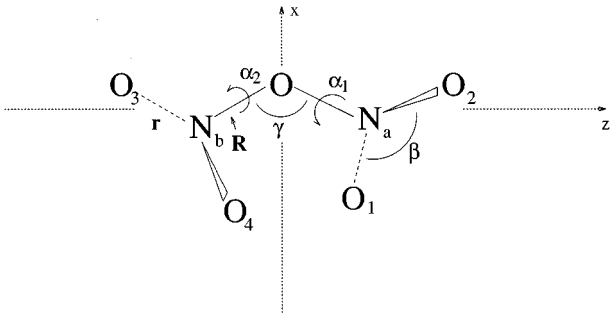

FIG. 1. Electron-diffraction geometry for N_2O_5 and the coordinate system used to discuss the structural analysis. The electron-diffraction geometry of McClelland *et al.* (Ref. 7) has $\alpha=\alpha_1=\alpha_2=30°$ $r=1.183(2)$ Å, $R=1.492(4)$ Å, $\gamma=111.8(16)°$, and $\beta=133.2(6)°$.

give a nearly planar configuration, with out of plane dihedral angles of ~22°, compared to the electron-diffraction angles of ~30°.[7] In addition, the density functional calculations predict a small electric-dipole moment for the molecule of 0.1–0.3 D, significantly less than the dielectric-constant measured value of 1.4 D for N_2O_5 in carbon tetrachloride solvent.[10]

Recently, Colmont,[5] guided by the electron-diffraction results, has reported the observation of the microwave spectrum of N_2O_5 using source frequency modulation with a waveguide sample cell. A near rigid-rotor series of lines were assigned to N_2O_5 based on a fit to a Watson[11] asymmetric-top Hamiltonian to a root-mean-square deviation of ~1.1 MHz, or about ten times the measurement uncertainty. Efforts were made to remove possible nitric acid impurities arising from the reaction of N_2O_5 with water, by comparing the observed spectrum with a HNO_3 spectrum obtained under similar conditions. Surprisingly, no direct evidence was obtained for tunneling splittings arising from large-amplitude motions, or for ^{14}N nuclear quadrupole hyperfine structure, presumably because of the high-J data sampled ($J \geqslant 15$).

In the present study we have examined the microwave spectrum of N_2O_5 between 8–25 GHz at a rotational temperature of ~2.5 K using the high sensitivity and high resolution (~2 kHz) of a pulsed-molecular-beam Fourier-transform microwave spectrometer. Definitive rotational assignments of the transitions are made by modeling the J-dependent nuclear quadrupole hyperfine patterns. The spectrum reveals two essentially equal-intensity asymmetric-rotor-like series, each poorly fit to a Watson Hamiltonian. The hyperfine patterns show that the two nitrogen nuclei sample equivalent chemical environments on a time scale faster than ~1 μs.

The observed nuclear-spin statistical weights require that the equilibrium nuclear configuration of N_2O_5 has a twofold axis of symmetry, in agreement with the electron-diffraction results. Model dynamical calculations and new high-level *ab initio* results described here, lead us to assign the two states to two tunneling components of a C_2 symmetry N_2O_5. The observed splittings are consistent with a tunneling pathway corresponding to a geared internal rotation of the two NO_2 groups about their C_2 axes. The present results suggest that the microwave spectrum of Colmont *et al.*[5] arises either from an excited state of N_2O_5 or from impurities.

II. EXPERIMENT

A. Measurements

Nitrogen pentoxide was synthesized by dehydrating dry nitric acid with phosphorous pentoxide, following the procedure of Caesar and Goldfrank[12] and others.[13] The reaction product was distilled, with the vapor collected in a stream of oxygen and ozone to insure complete oxidation of any NO_2 byproduct to N_2O_5. Care was taken to avoid introduction of water vapor into the system since N_2O_5 is rapidly converted to nitric acid in the presence of water. The purity of the resulting product was periodically tested using Fourier-transform infrared spectroscopy.

The Balle–Flygare pulsed-nozzle Fourier-transform spectrometer[14] used in the present investigation has been described previously.[15] To increase the sensitivity and resolution, we follow Grabow and Stahl,[16] and direct the nozzle pulse down the cavity axis. In this configuration each of the transitions appears as a doublet, separated by 50–75 kHz symmetrically about the line center. In a frequency-domain picture these doublets occur because of the opposite Doppler shifts of the two electromagnetic waves emitted parallel and antiparallel to the direction of the molecular-beam propagation. In a time-domain picture, the doublets arise from the modulation of the electromagnetic field due to the motion of the macroscopic dipole moment of the inhomogeneously polarized molecular beam through the TEM_{plq} mode pattern of the resonator. The moving macroscopic dipole moment causes a modulation of the electromagnetic field equivalent to the splitting observed in the frequency domain.

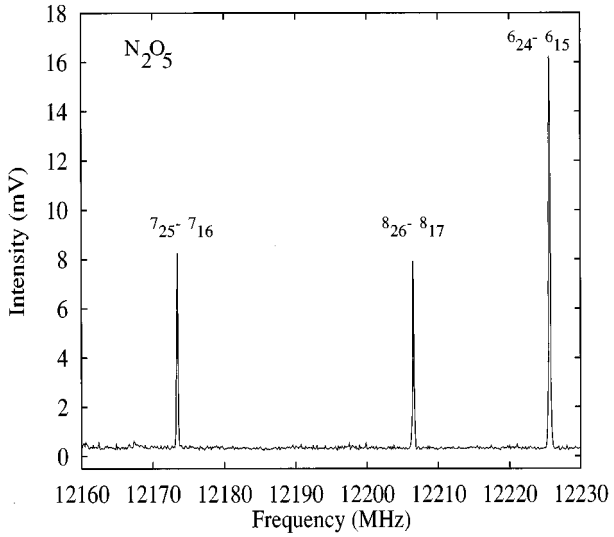

FIG. 2. Low-resolution survey spectrum for N_2O_5 showing the three J components of the $K_a=2-1$, Q branch for the A_1^- state. The spectrum was acquired in ~45 min.

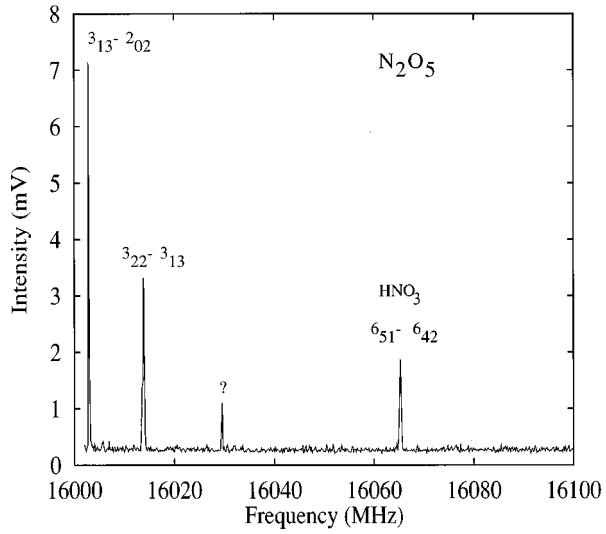

FIG. 3. Low-resolution survey spectrum for N_2O_5 showing the 3_{13}–2_{02} and 3_{22}–3_{13} transitions for the A_1^+ state and the 6_{51}–6_{42} impurity transition for HNO_3.

A molecular beam of N_2O_5 was formed by flowing, at a pressure of ~115 kPa, a mixture of ~20% by volume He in Ne over N_2O_5 solid at −20 to 0 °C through a 1 mm diameter pulsed-nozzle valve[17] using a glass and Teflon gas manifold. Low-resolution (0.2–0.5 MHz) broadband survey spectra were recorded between 8.82–9.02, 9.814–11.423, 11.500–17.488, 17.665–19.225, and 21.055–22.378 GHz as described by Andresen *et al.*[18] Sample low-resolution survey spectra are shown in Figs. 2 and 3, and a sample high-resolution spectrum is shown in Fig. 4. The main contaminant lines in the spectra are due to nitric acid originating from the hydration reaction of the N_2O_5 with residual water vapor in the gas-handling system.

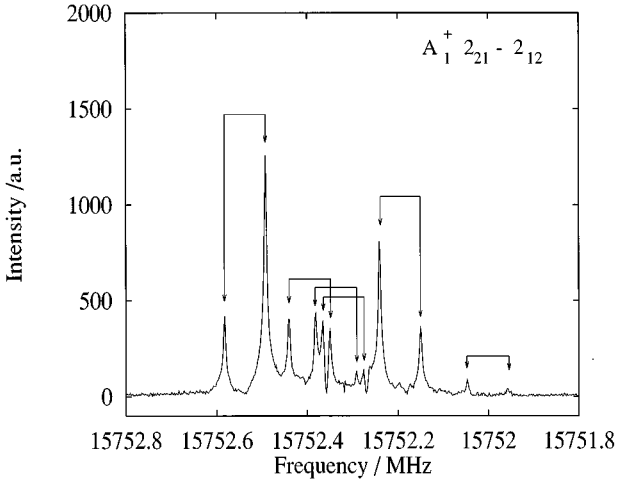

FIG. 4. High-resolution spectrum of the 2_{21}–2_{12} transition for the A_1^+ state of N_2O_5. The hyperfine pattern arises from the two $I=1$ ^{14}N quadrupolar nuclei giving a resultant nitrogen nuclear spin of 1. The arrows point out the ''Doppler doublets.''

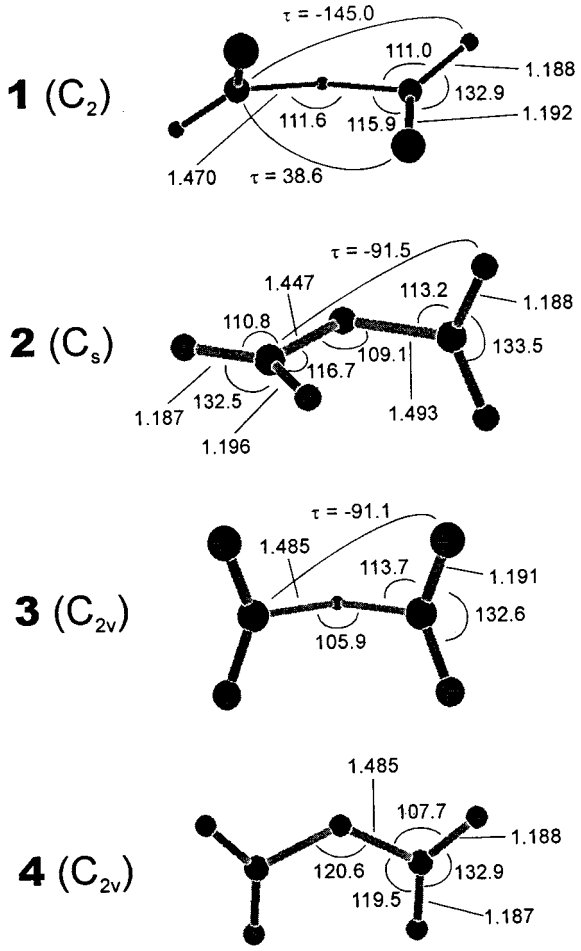

FIG. 5. Geometries of four conformations of N_2O_5 optimized at the QCISD/6-311G* level (active core) under the symmetry constraints indicated.

B. *Ab initio* calculations

Four conformations were considered computationally. Structures **1, 2, 3**, and **4** correspond approximately to the (α_1,α_2) torsional coordinate values (α,α), (0,90°) or (90°,0), (90°,90°), and (0,0), respectively. These conformations belong to the point groups C_2, C_s, C_{2v}, and C_{2v}, respectively (see Fig. 5). Geometries for all four conformations were fully optimized within the appropriate symmetry restrictions, without constraining the O–NO_2 moieties to be planar. Because of the point-group restrictions, however, the optimized geometries do not necessarily represent minima on the corresponding potential energy surfaces. Geometries, relative energies, and dipole moments were determined at the HF/6-311G*, MP2/6-311G* (active core), QCISD/6-311G* (active core), SVWN/6-311G*, BLYP/6-311G*, and Becke3LYP/6-311G*. The last three are density functional methods and were included to aid comparison with a prior density functional study of N_2O_5.[9] SVWN is local, employing Slater's exchange functional ($\alpha=2/3$)[19] and the Vosko–Wilk–Nusair correlation functional.[20] BLYP includes the nonlocal (gradient) corrections to the exchange and correlation functionals due to Becke[21] and to Lee, Yang, and Parr,[22]

TABLE I. Transition line centers and effective nuclear quadrupole coupling constants for N_2O_5 in MHz.[a,b]

$J'_{K_aK_c}-J''_{K_aK_c}$	$\nu_0(A_1^+)$	eQq'_{eff}	eQq''_{eff}	$\nu_0(A_1^-)$	eQq'_{eff}	eQq''_{eff}
$1_{11}-0_{00}$	9 171.278 78(92)	0.1900(23)	⋯	⋯	⋯	⋯
$2_{12}-1_{01}$	12 658.155 06(41)	−0.4349(19)	−0.6406(16)	11 190.263 22(46)	−0.4402(22)	−0.6063(18)
$3_{13}-2_{02}$	16 002.971 40(91)	−0.5978(39)	−0.6468(31)	14 736.326 57(42)	−0.6031(18)	−0.6140(15)
$4_{14}-3_{03}$	19 220.199 94(97)	−0.6703(49)	−0.6404(54)	18 218.538 2(13)	−0.6563(64)	−0.6352(68)
$5_{15}-4_{04}$	22 331.870 18(84)	−0.6933(37)	−0.6619(51)	21 636.5(2)	⋯	⋯
$6_{16}-5_{05}$	25 367.586 6(18)	Δ=	−0.031(10)	⋯	⋯	⋯
$4_{04}-3_{13}$	10 381.773 83(66)	−0.663(17)	−0.594(17)	11 186.355 11(28)	−0.6369(11)	−0.6008(12)
$5_{05}-4_{14}$	14 604.645 (5)	⋯	⋯	15 069.303 0(23)	−0.665(12)	−0.649(13)
$6_{15}-5_{23}$	⋯	⋯	⋯	10 961.705 22(22)	−0.509(18)	−0.426(18)
$7_{16}-6_{24}$	⋯	⋯	⋯	14 382.2(2)	⋯	⋯
$7_{17}-6_{25}$	⋯	⋯	⋯	11 563.1(1)	⋯	⋯
$2_{20}-2_{11}$	14 957.879 84(62)	0.6383(20)	−0.2089(18)	12 791.831 04(91)	0.6302(29)	−0.1841(29)
$3_{21}-3_{12}$	14 466.829 1(10)	0.0[c]	−0.3896(54)	12 648.242 40(96)	0.0[c]	−0.3542(50)
$4_{22}-4_{13}$	13 876.9524 7(45)	−0.2265(18)	−0.4317(16)	12 489.265 08(33)	−0.2441(13)	−0.4171(11)
$5_{23}-5_{14}$	13 235.854 6(10)	Δ=	+0.12504(50)	12 339.551 90(10)	Δ=	+0.0996(50)
$6_{24}-6_{15}$	12 597.807 8(12)	Δ=	+0.0768(42)	12 225.642 95(62)	−0.4136(23)	−0.4667(25)
$7_{25}-7_{16}$	12 021.017 78(97)	Δ=	+0.0655(54)	12 173.439 88(62)	Δ=	+0.0330(31)
$8_{26}-8_{17}$	11 563.1(1)	⋯	⋯	12 206.5(1)	⋯	⋯
$9_{27}-9_{18}$	⋯	⋯	⋯	12 345.879 58(57)	Δ=	+0.0387(29)
$10_{28}-10_{19}$	⋯	⋯	⋯	12 611.56(3)	⋯	⋯
$11_{29}-11_{1,10}$	⋯	⋯	⋯	13 024.21(1)	⋯	⋯
$2_{21}-2_{12}$	15 752.271 51(96)	0.6357(45)	−0.4373(45)	13 357.684 49(67)	0.6292(31)	−0.4410(31)
$3_{22}-3_{13}$	16 013.863 03(79)	0.0[c]	−0.6057(28)	13 757.239 65(61)	0.0[c]	−0.5911(20)
$4_{23}-4_{14}$	16 369.835 15(82)	−0.2478(46)	−0.6685(46)	14 288.619 06(76)	−0.2517(41)	−0.6563[c]
$5_{24}-5_{15}$	16 826.370 74(58)	−0.3765(28)	−0.7004(22)	14 950.469 81(64)	−0.3939(30)	−0.7037(28)
$6_{25}-6_{16}$	17 390.775 28(50)	Δ=	+0.2693(28)	15 740.621 975(85)	Δ=	+0.25564(47)
$7_{26}-7_{17}$	18 070.759 09(54)	Δ=	+0.2363(19)	16 655.643 0(12)	−0.5178(57)	−0.7377(62)
$8_{27}-8_{18}$	⋯	⋯	⋯	17 690.478 16(15)	Δ=	+0.20289(86)

[a]Experimental uncertainties are one standard deviation as determined by a least squares fit of each rotational transition to a line center and one or two quadrupole coupling constants.
[b]$\Delta = eQq'_{\text{eff}} - eQq''_{\text{eff}}$.
[c]Constrained in the fit.

respectively. Becke3LYP (also called B3LYP) is similar, but also includes the HF density in a parameterized way.[23] It is closely related to the three-parameter functional that Becke optimized for the thermochemistry of small molecules.[24] Vibrational analysis (stationary point characterization) was done only at the HF and MP2 levels. Relative energies of the four conformations were also computed at the CCSD(T)/6-311G*, frozen-core CCSD(T)/6-311G*, and frozen-core CCSD(T)/6-311+G* levels, in all these cases using the QCISD/6-311G* geometries.

The electric-field gradient was computed at the nitrogen nuclei at the QCISD//QCISD/6-311G* level. To calibrate the accuracy of these results, the analogous calculation was done for nitric acid (HNO_3), for which experimental results are available.[25] Further test calculations on HNO_3, using lower levels of theory and both larger and smaller basis sets, showed that the orientation of the principal axes of the field-gradient tensor is insensitive to these computational details, as has been found previously.[26]

The *d*-type polarization functions were used in spherical form (5D) for all calculations except the QCISD geometry optimizations and electric-field gradients, in which case software restrictions required the Cartesian form (6D). All electrons were active in correlated calculations unless otherwise indicated. Computations were done using the GAUSSIAN 92/DFT,[27] GAUSSIAN 94,[28] and ACES II[29,30] program packages.[31]

III. RESULTS

A. Microwave spectrum

1. Rotational analysis

The observed transitions for N_2O_5 corrected for hyperfine splittings are listed in Table I. A complete set of the measured transitions which include the frequencies of the individual hyperfine components is available from PAPS.[32] Two sets of essentially equal intensity *b*-type asymmetric-rotor-like transitions are observed, assigned to two internal-rotor/tunneling states of the molecule, denoted A_1^+ and A_1^- in the table. Since collisional relaxation is allowed between the two tunneling states, the nearly equal intensity of the two sets of transitions indicates that the energy difference between the two states must be small compared to the molecular-beam temperature of ~2.5 K≡52 GHz. The large number of other internal-rotor states possible for a system with two tops are not observed, either because they are not populated due to the cold molecular-beam temperature, or because they cannot exist due to the Bose–Einstein statistics of the spin-zero oxygen nuclei being interchanged by the internal rotation. Transitions are observed for the $K_a=2-1$

and 1–0 subbands of the two states, for J levels up to 11. No evidence was found for transitions between the two states, presumably because these transitions are either too weak or forbidden. We note that the ''permanent'' b-type dipole moment component itself must be small, less than ~0.5 D, as estimated by the amount of power needed to create a $\pi/2$ polarizing pulse.

Attempts to fit the rotational series of either of the internal-rotor/tunneling states to a Watson[11] asymmetric-rotor Hamiltonian proved unsuccessful. Because the hyperfine analysis discussed below definitively establishes the J and K_a quantum numbers of the transitions, it is improbable that misassigned transitions are responsible for our inability to fit the transitions to an asymmetric-rotor Hamiltonian. More likely, the rotational progressions are strongly affected by the internal rotation of the NO_2 groups. In the high internal-rotation-barrier limit, the rotational transitions of the two observed internal states for the same set of rotational quantum numbers will converge to the same frequency. However, we observe large splittings of the rotational transitions. For instance, the 2_{12}–1_{01} transitions for the two states are separated by ~1.5 GHz, while the 2_{21}–2_{12} transitions are separated by ~2.4 GHz.

If we apply a rigid asymmetric rotor analysis and assume that the 2_{12}–1_{01} transition occurs at $A+3C$ and the 2_{21}–2_{12} transition occurs at $3(A-C)$, we find that the A and C rotational constants are approximately 7103 and 1852 MHz for the A_1^+ state and 6137 and 1684 MHz for the A_1^- state. The effect of nonrigidity is seen by noting that these A and C values for the A_1^+ state predict the 1_{11}–0_{00} transition at ~8955 MHz (i.e., $A+C$) compared to the observed value of 9171 MHz. The apparent B rotational constants for the two states are also significantly different. The $K=0$ combination differences from the $K_a=1-0$ subband yield an approximate $(B+C)/2$ value for the A_1^+ state of 1894 MHz, corresponding to a B value of ~1936 MHz, and an approximate $(B+C)/2$ value for the A_1^- state of 1855 MHz, corresponding to a B value of ~2026 MHz.

2. Hyperfine analysis

The $I=1$, ^{14}N quadrupole hyperfine structure allows definitive assignments of the J and K_a quantum numbers to the transitions and provides information about the geometry of the molecule. The observed quadrupole hyperfine structure is characteristic of two equivalent quadrupolar nuclei, demonstrating that N_2O_5 has two different nuclear-spin modifications. For both internal-rotor/tunneling states, rotational states with K_a+K_c even have a resultant nitrogen nuclear spin of $I_N=0,2$, while rotational states with K_a+K_c odd have $I_N=1$. This fact implies that in the high-barrier limit when the two tunneling states become degenerate, states with K_a+K_c even and K_a+K_c odd will have different nuclear spins. The presence of two different spin modifications in the high-barrier limit requires that the equilibrium configuration of the molecule has a twofold axis of symmetry.

For each transition, the hyperfine patterns were fit to the frequencies calculated from the energy-level expression[33]

$$H=H_{\mathrm{rt}}+H_Q(\mathbf{I}_1,\mathbf{J})+H_Q(\mathbf{I}_2,\mathbf{J}), \tag{1}$$

where

$$H_Q(I_i,J)=\frac{(eQq_J)_i}{2I_i(2I_i-1)J(2J-1)} \times[3(\mathbf{I}_i\cdot\mathbf{J})^2+\tfrac{3}{2}(\mathbf{I}_i\cdot\mathbf{J})-\mathbf{I}_i^2\mathbf{J}^2]. \tag{2}$$

Here, H_{rt} is the rotation–internal-rotation Hamiltonian, $\mathbf{I}_i$ is the nuclear-spin angular momentum of the ith nitrogen nucleus, and $(eQq_J)_i$ is the coupling constant of the ith nitrogen nucleus and is a characteristic of a particular rotation–internal-rotation state. Because the two nitrogen nuclei are equivalent, only the average of the $(eQq_J)_i$, $(eQq_J)_{\mathrm{ave}}=[(eQq_J)_1+(eQq_J)_2]/2$, is determined for a particular rotation-internal-rotation state. The eigenvalues of H are evaluated in the energy representation of H_{rt}, with the quadrupole interaction treated by first-order perturbation theory in this basis. In the initial analysis of the hyperfine interactions, no explicit knowledge of H_{rt} is required; each observed transition is fit to a hyperfine-free line center and two average quadrupole coupling constants, $(eQq_J)_{\mathrm{ave}}$, one for the upper state and the other for the lower state. The $(eQq_J)_{\mathrm{ave}}$ were scaled by $(2J+3)/J$ for $J\neq 0$ to remove the J dependence from the constants. The resulting effective average coupling constants for each state, eQq_{eff} are listed in Table I next to the hypothetical hyperfine-free line centers.

The eQq_{eff} for the 1_{01}, 1_{11}, 1_{10}, 2_{12}, 2_{11}, and 2_{21} states are related to the components of the quadrupole coupling tensor along the principal inertial axes, eQq_{aa}, eQq_{bb}, and eQq_{cc}, averaged over the two nuclear environments. For the 1_{01}, 1_{11}, 1_{10}, 2_{12}, 2_{11}, and 2_{21} states the eQq_{eff} are equal to $-eQq_{aa}$, $-eQq_{bb}$, $-eQq_{cc}$, eQq_{cc}, eQq_{bb}, and eQq_{aa}, respectively, independent of the asymmetry parameter, κ. This approximation breaks down if the two internal-rotor/tunneling states are interacting with each other or with other states through Coriolis interactions, since, for example, a state which correlates with a 1_{01} state may now be an admixture of 1_{01} and 1_{10} character due to a b-type Coriolis interaction operating between the two tunneling states. From an analysis of the hyperfine structure of transitions involving the 1_{01}, 1_{11}, 1_{10}, 2_{12}, 2_{11}, and 2_{21} states we obtain $eQq_{aa}=0.6291(54)$ MHz, $eQq_{bb}=-0.1948(59)$ MHz, and $eQq_{cc}=-0.4343(80)$ MHz. For an unperturbed vibrational or internal-rotor/tunneling state, $eQq_{aa}+eQq_{bb}+eQq_{cc}=0$, for eQq_{ii} determined in this manner. Equivalently, the eQq_{eff} for all the K_aK_c components of a given J sum to zero within a tunneling or vibrational state. Both of these conditions are violated by the coupling constants listed in Tables I. For $J=2$ of the A_1^+ state, the eQq_{eff}'s sum to $-0.0178(65)$ MHz, while for the A_1^- state they sum to 0.0316(58) MHz. If we add these sums for the two internal-rotor states, we obtain a value of 0.0138(87) MHz, which is effectively zero for an uncertainty of two standard deviations. This result suggests that the two internal-rotor states are interacting via Coriolis interactions, redistributing the quadrupole coupling constant components between them.

In addition to guiding the rotational assignment, the ^{14}N quadrupole hyperfine structure provides precise structural in-

formation on N_2O_5. To obtain this information, we first assume that the electric-field-gradient tensors at the two nitrogen nuclei are similar to that found in HNO_3. *Ab initio* calculations presented in the next section support this assumption. Making this approximation allows us to calculate the components of the electric field gradient, and thus of the quadrupole coupling constant, along the principal inertial axis system of N_2O_5 by projecting the quadrupole tensor of the individual NO_2 groups onto the inertial frame. These projections are principally a function of the NO_2 torsional angles, α_1 and α_2, and the NON valence angle, γ, defined in Fig. 1. Because experimentally we observe that the two nitrogen nuclear environments are dynamically equivalent, we average the projections of the two NO_2 groups before comparing with experiment. The angles α_1 and α_2 are referenced to the planar configuration, where $\alpha_1=0$ and $\alpha_2=0$. $\alpha_1=\alpha_2$ corresponds to a C_2 symmetry structure, $\alpha_1=180°-\alpha_2$, $\alpha_1=0$, $\alpha_2=90°$, and $\alpha_1=90°$, $\alpha_2=0$ correspond to C_s symmetry structures, and $\alpha_1=\alpha_2=90°$ corresponds to a C_{2v} symmetry structure. We assume that the two NO_3 groups are planar and equivalent and fix the NO bond lengths and NO_2 angles at the electron-diffraction values:[7] $r=1.183(2)$ Å, $R=1.492(4)$ Å, and $\beta=133.2(6)°$. Essentially identical results are obtained if we use the *ab initio* values for r, R, and β, presented below.

The principal axes of the quadrupole coupling tensors of the two nitrogen nuclei are approximated by placing an (x,y,z) axis systems on each of the two NO_2 groups with the z-axes fixed normal to the NO_2 planes and the x axes fixed along the NO bonds which form the NON backbone. For HNO_3, Albinus *et al.*[25] have found this to be an accurate representation of the orientation of the principal-axis system; the x axis of the principal-axis system of HNO_3 is rotated by only 1.1° from the unique NO bond axis. Our *ab initio* calculations discussed later support the assumption that the principal-axis system of the electric-field gradient tensor of N_2O_5 has one component along the NO bond of the NON backbone and distorts minimally with changes in the internal rotation angle. Thus for N_2O_5 we approximate the two quadrupole coupling tensors by $eQq_{zz}=-0.070$ MHz, $eQq_{xx}=+1.103$ MHz, and $eQq_{yy}=-1.033$ MHz, the principal axis system components of HNO_3.[25]

Guided in part by the electron diffraction results and the *ab initio* calculations discussed below, we examine the predicted quadrupole coupling constants for three types of structures: a C_2 configuration with $\alpha=\alpha_1=\alpha_2$, a C_{2v} structure with $\alpha=\alpha_1=\alpha_2=0$ or 90°, and a C_s structure with $\alpha_1=0$, $\alpha_2=90°$, or equivalently, $\alpha_1=90°$, $\alpha_2=0$. The results for possible C_2 and C_{2v} configurations are shown in Fig. 6, where we plot calculated values for the quadrupole coupling constants, eQq_{aa}, eQq_{bb}, and eQq_{cc}, as a function of α for three values of the N–O–N angle, $\gamma=110.0°$, 120.5°, and 130.0°. Recall for the electron-diffraction results $\gamma=111.8(6)°$ and for the *ab initio* calculations $\gamma=103°$–123°, depending on level of theory and values of α_1 and α_2. The solid horizontal lines give the three experimental values for the coupling constants [$eQq_{aa}=0.6291(54)$ MHZ, $eQq_{bb}=-0.1948(59)$ MHz, and $eQq_{cc}=-0.4343(80)$ MHz], taken by averaging the relevant results in Table I. The two solid vertical lines in the figure show the values of α

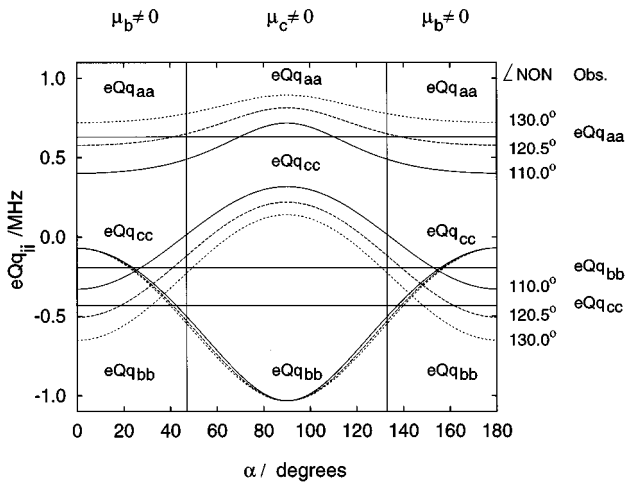

FIG. 6. Plot of calculated eQq_{aa}, eQq_{bb}, and eQq_{cc} as a function of torsion angle, $\alpha=\alpha_1=\alpha_2$ for three values for the NON angle, γ, using the model discussed in the text. The experimental values for the coupling constants are represented by the three horizontal lines in the figure. The two vertical lines show the values of α where the electric-dipole selection rules change from b type to c type. The best agreement between the calculated and observed values occurs for $\alpha=41°$ and γ 120.5°.

TABLE II. Estimated quadrupole coupling constants for various geometries of N_2O_5 in MHz.

α_1	α_2	∠NON	eQq_{aa}	eQq_{bb}	eQq_{cc}
0°	0°	110°	0.4003	−0.3303	−0.0700
		120°	0.5690	−0.4990	−0.0700
		130°	0.7215	−0.6515	−0.0700
0°	90°	110°	0.5091	0.0424	−0.5515
		120°	0.6504	−0.0989	−0.5515
		130°	0.7790	−0.2275	−0.5515
90°	90°	110°	0.7171	−1.0330	0.3159
		120°	0.8097	−1.0330	0.2233
		130°	0.8935	−1.0330	0.1395
Experiment			0.6291(54)	−0.1948(59)	−0.4343(80)

TABLE III. Computed and experimental geometries and dipole moments (μ) for conformations **1–4** of N_2O_5 (C_2, C_s, C_{2v}, and C_{2v} symmetry, respectively) with all electrons active and the 6-311G* basis set. Terminal dihedral angles (N–O–N–O) are denoted by the symbol τ. Other parameters are defined in Fig. 1. For conformation **1**, the average angles $\alpha_1=\alpha_2=\alpha\equiv(\tau_1+180°+\tau_2)/2$.

	B3LYP				QCISD				
Parameter	**1**	**2**	**3**	**4**	**1**	**2**	**3**	**4**	Expt.[a]
R_a (Å)		1.568				1.493			
	1.513		1.531	1.525	1.470		1.485	1.485	1.498
R_b (Å)		1.460				1.447			
r_1 (Å)		1.182				1.188			
	1.188			1.185	1.192			1.187	
r_4 (Å)		1.198				1.196			
			1.188				1.191		1.188[b]
r_2 (Å)		1.182				1.188			
	1.199			1.186	1.188			1.188	
r_3 (Å)		1.190				1.187			
β_a (°)		134.9				133.5			
	133.8		133.3	133.5	132.9		132.6	132.9	133.2
β_b (°)		132.2				132.5			
γ (°)	115.3	110.1	107.3	120.9	111.6	109.1	105.9	120.6	111.8
τ_1 (°)		91.5				91.5			
	30.7		91.2	0.0	38.6		91.1	0.0	~30[b]
τ_4 (°)		0.0				0.0			
τ_2 (°)		−91.5				−91.5			
	−151.3		−91.2	180.0	−145.0		−91.1	180.0	~−150[b]
τ_3 (°)		180.0				180.0			
α_1 (°)		90.0				90.0			
	29.7		90.0	0.0	36.8		90.0	0.0	~30
α_2 (°)		0.0				0.0			
μ (D)[c]	0.03	0.78	0.03	0.25	0.24	0.43	0.21	0.17	1.39

[a]Geometry (conformation **1**) from Ref. 7 and dipole moment (in CCl_4 solution) from Ref. 10.
[b]Local C_{2v} symmetry was assumed in Ref. 7.
[c]$1D=3.3357\times10^{-30}$ C m.

($47\pm1°$ and $133\pm1°$) where the b and c inertial axes switch for the N–O–N angles considered. The b and c axis switching arises due to the definition of rotational constants which requires that $A>B>C$, and leads to a flipping of the selection rules from b-type ($\mu_b\neq0$) to c type ($\mu_c\neq0$). As seen in the figure, the calculated quadrupole coupling constants are a sensitive function of α. The best agreement with experiment is obtained for $\alpha=41°$ and $\gamma=120.5°$ with 1σ uncertainties of less than 1° on each angle. These choices of angles predict b-type selection rules, as observed experimentally.

Only the C_2 configuration discussed above is consistent with the observed quadrupole coupling constants. This is seen in Fig. 6 where we give calculated eQq's for the two possible C_{2v} configurations ($\alpha=0$ or $\alpha=90°$) and in Table II where we compare these configurations with the C_s configuration ($\alpha_1=0$, $\alpha_2=90°$ or $\alpha_1=90°$, $\alpha_2=0$). The experimental results are clearly inconsistent with a C_{2v} or C_s geometry for the molecule. In particular, for the C_s configuration the calculated value for eQq_{cc} is −0.5515 MHz, independent of γ, and differs significantly from the observed value of −0.4343(80) MHz.

B. *Ab initio* calculations

The computed geometries and dipole moments for structures **1–4** are summarized in Table III. For conciseness, only the results from the B3LYP and QCISD calculations are listed; the results from the HF, SVWN, BLYP, and MP2 calculations may be obtained directly from the authors. Figure 5 shows the optimized geometries for structures **1–4** at our highest level of theory (QCISD). The deviation from planarity of the $O–NO_2$ groups, defined as the supplement of the dihedral angle between terminal oxygen atoms, is 3.6°, 3.0° (for the out-of-plane group), 2.2°, and 0° (by symmetry) for structures **1–4**, respectively. The computed relative energies, without any corrections for vibrational zero-point energy, are collected in Table IV. The numbers of imaginary vibrational frequencies obtained for structures (**1,2,3,4**) are (1,0,2,1) and (0,0,2,2) at the HF/6-311G* and MP2/6-311G* levels, respectively. For structure **1** (C_2 symmetry), which is the one determined experimentally,[7] the computed vibrational frequencies and infrared intensities are listed in Table V.

Electric field gradients at the nitrogen nuclei were characterized by the angle formed between the chemically unique N–O bond and the nearest principal axis of the electric-field gradient tensor. For HNO_3, the computed angle is 0.3°, indicating that the $N–O_H$ bond lies along a principal axis of the electric-field gradient tensor. This value compares favorably with the experimental angle of 1.1°.[7] For N_2O_5, the computed angles are 7.2°, 1.3°, 2.4°, and 4.2° for structures **1–4**, respectively.

TABLE IV. Computed relative energies in cm^{-1} for conformations **1–4**. The 6-311G* basis set was used and all electrons were active in correlated calculations, except as noted.

Calculation	Relative energy of conformation			
	1	**2**	**3**	**4**
HF	0.0	−28.6	2751.4	1508.2
MP2	0.0	−82.4	2242.7	583.5
SVWN	0.0	265.5	3360.5	174.0
BLYP	0.0	288.5	2630.3	81.7
B3LYP	0.0	120.4	2484.7	380.1
QCISD	0.0	−8.2	2312.4	1065.4
CCSD(T)[a]	0.0	−35.6	2188.9	868.4
val-CCSD(T)[a,b]	0.0	−29.2	2172.9	863.8
val-CCSD(T)[a,b,c]	0.0	154.5	2400.7	1176.0

[a]Using the QCISD/6-311G* geometry.
[b]Frozen-core; only valence electrons correlated.
[c]Using the 6-311+G* basis set.

TABLE V. Computed vibrational frequencies in cm^{-1} and infrared intensities in km/mol for conformation **1** (C_2 symmetry) of N_2O_5. The HF and MP2 frequencies have been scaled by 0.90 and 0.95, respectively.

Symm.	HF/6-311G*		MP2/6-311G*	
	Freq.	Int.	Freq.	Int.
A	1801	681.8	1879	182.8
A	1451	82.3	1303	48.5
A	974	17.0	822	45.0
A	879	12.7	767	1.1
A	712	7.4	631	2.3
A	461	0.5	347	3.3
A	247	2.4	213	0.3
A	81	0.8	64	0.3
B	1757	1005.6	1861	178.8
B	1344	381.4	1224	289.5
B	893	709.7	719	217.3
B	787	90.6	690	30.0
B	767	17.4	519	233.2
B	528	22.1	226	574.6
B	7*i*	0.8	18	13.8

C. Internal-rotation theory

In the present section we present a dynamical model which allows the calculation of the rotational-tunneling spectrum of N_2O_5 for a given structure and torsional potential. We start with a group theoretical discussion of N_2O_5 using the molecular-symmetry group of Longuet–Higgins.[34] A model Hamiltonian is developed which treats all the internal modes as rigid except for the two NO_2 torsions. Diagonalization of the associated Hamiltonian matrix is facilitated by using symmeterized basis functions to factor the matrix. As shown below, the resulting calculations give insight into the nature of the two internal-rotor/tunneling states observed for N_2O_5.

Allowing internal-rotation of the two NO_2 groups, the most general molecular symmetry group for N_2O_5 is G_{16}. This group has been previously applied to help interpret the large-amplitude motions observed in the water dimer.[35] The character table for G_{16} is shown in Table VI,[35] where the permutation-inversion operations use the numbering of the nuclei as given in Fig. 1. For a noninternally rotating or tunneling N_2O_5 with a C_2 minimum, such as found in the electron diffraction and hyperfine analysis, each rotation–vibration state is eightfold degenerate, corresponding to the eight configurations pictured in Fig. 7. Tunneling between the eight minima lifts the eightfold degeneracy. Starting from a single reference configuration, four of the minima are sampled by a geared rotation of the two NO_2 groups about their C_2 axes as pictured in Fig. 8. An antigeared inversion of each of these configurations through either a planar or nonplanar C_{2v} transition state, also shown in Fig. 8, allows access to the other four minima. The vibrational wave functions for the eight configurations generates an eight-dimensional reducible representation of G_{16} as $A_1^+ \oplus A_1^- \oplus B_2^+ \oplus B_2^- \oplus E^+ \oplus E^-$. Thus tunneling between all the eight configurations of Fig. 7 will split the $J=0$ vibrational state into six tunneling sublevels of A_1^+, A_1^-, B_2^+, B_2^-, E^+, and E^- symmetry.

The qualitative effects of tunneling between the eight minimum can be gleaned by constructing a tunneling Hamiltonian matrix for a $J=0$ N_2O_5

TABLE VI. Character table for the G_{16} molecular symmetry group used for N_2O_5.

	E	(12)(34)	(12) (34)	$(ab)(14)(23)$ $(ab)(13)(24)$	$(ab)(1324)$ $(ab)(1423)$	E^*	(12)(34)*	(12)* (34)*	$(ab)(14)(23)^*$ $(ab)(13)(24)^*$	$(ab)(1324)^*$ $(ab)(1423)^*$
A_1^+	1	1	1	1	1	1	1	1	1	1
A_2^+	1	1	−1	−1	1	1	1	−1	−1	1
B_1^+	1	1	1	−1	−1	1	1	1	−1	−1
B_2^+	1	1	−1	1	−1	1	1	−1	1	−1
E^+	2	−2	0	0	0	2	−2	0	0	0
A_1^-	1	1	1	1	1	−1	−1	−1	−1	−1
A_2^-	1	1	−1	−1	1	−1	−1	1	1	−1
B_1^-	1	1	1	−1	−1	−1	−1	−1	1	1
B_2^-	1	1	−1	1	−1	−1	−1	1	−1	1
E^-	2	−2	0	0	0	−2	2	0	0	0

$$
\begin{array}{c}
 \\ \phi_1 \\ \phi_2 \\ \phi_3 \\ \phi_4 \\ \phi_5 \\ \phi_6 \\ \phi_7 \\ \phi_8
\end{array}
\begin{array}{c}
\begin{array}{cccccccc} \phi_1 & \phi_2 & \phi_3 & \phi_4 & \phi_5 & \phi_6 & \phi_7 & \phi_8 \end{array} \\
\left[\begin{array}{cccccccc}
E_0 & -|h_g| & 0 & -|h_g| & -|h_n| & -|h_i| & -|h_p| & -|h_i| \\
-|h_g| & E_0 & -|h_g| & 0 & -|h_i| & -|h_n| & -|h_i| & -|h_p| \\
0 & -|h_g| & E_0 & -|h_g| & -|h_p| & -|h_i| & -|h_n| & -|h_i| \\
-|h_g| & 0 & -|h_g| & E_0 & -|h_i| & -|h_p| & -|h_i| & -|h_n| \\
-|h_n| & -|h_i| & -|h_p| & -|h_i| & E_0 & -|h_g| & 0 & -|h_g| \\
-|h_i| & -|h_n| & -|h_i| & -|h_p| & -|h_g| & E_0 & -|h_g| & 0 \\
-|h_p| & -|h_i| & -|h_n| & -|h_i| & 0 & -|h_g| & E_0 & -|h_g| \\
-|h_i| & -|h_p| & -|h_i| & -|h_n| & -|h_g| & 0 & -|h_g| & E_0
\end{array}\right]
\end{array}, \tag{3}
$$

where ϕ_1–ϕ_8 are the vibrational wave functions for the eight different configurations of Fig. 7, $|h_g|$ is a tunneling matrix element describing the coupling between nearest neighbor minima for the geared internal rotation, $|h_p|$ is the corresponding matrix element for the antigeared inversion through a planar transitions state, $|h_n|$ is the tunneling matrix element for the antigeared inversion through a nonplanar C_{2v} transition state, and $|h_i|$ is a tunneling matrix element for the independent rotation of one of the NO_2 groups by 180°. The coefficients of these matrix elements are negative to insure that the totally symmetric state is lowest in energy. The eigenvalues and eigenvectors resulting from diagonalization of the matrix are

$$
\begin{array}{lll}
A_1^+ & (\phi_1+\phi_2+\phi_3+\phi_4+\phi_5+\phi_6+\phi_7+\phi_8)/\sqrt{8} & E_0-2|h_g|-|h_n|-|h_p|-2|h_i| \\
A_1^- & (\phi_1-\phi_2+\phi_3-\phi_4-\phi_5+\phi_6-\phi_7+\phi_8)/\sqrt{8} & E_0+2|h_g|+|h_n|+|h_p|-2|h_i| \\
B_2^+ & (\phi_1-\phi_2+\phi_3-\phi_4+\phi_5-\phi_6+\phi_7-\phi_8)/\sqrt{8} & E_0+2|h_g|-|h_n|-|h_p|+2|h_i| \\
B_2^- & (\phi_1+\phi_2+\phi_3+\phi_4-\phi_5-\phi_6-\phi_7-\phi_8)/\sqrt{8} & E_0-2|h_g|+|h_n|+|h_p|+2|h_i| \\
E^+ & (\phi_1-\phi_3+\phi_7-\phi_5)/\sqrt{4} & E_0-|h_n|+|h_p| \\
 & (\phi_2-\phi_4+\phi_8-\phi_6)/\sqrt{4} & E_0-|h_n|+|h_p| \\
E^- & (\phi_1-\phi_3-\phi_7+\phi_5)/\sqrt{4} & E_0+|h_n|-|h_p| \\
 & (\phi_2-\phi_4-\phi_8+\phi_6)/\sqrt{4} & E_0+|h_n|-|h_p|
\end{array}, \tag{4}
$$

where E_0 is the zero of energy for the degenerate nontunneling vibrational states. Figure 9 shows the predicted energy level diagram for the 0_{00} state under the assumption that the tunneling matrix elements have the size order $2|h_g|>|h_n|>|h_p|>2|h_i|$.

For the dominant isotopomer ($^{14}N_2{}^{16}O_5$) the total wave function must be of A_1^+ or A_1^- symmetry in G_{16}. Since the nuclear-spin functions transform as $6A_1^+ \oplus 3B_1^+$, only rovibronic states of A_1^+, A_1^-, B_1^+, and B_1^- symmetry are allowed. The $A_1^\pm$ states have a statistical weight of 6 (corresponding to a resultant N nuclear spin of $I_N=0,2$) and the $B_1^\pm$ states have a statistical weight of 3 (resultant N nuclear spin of $I_N=1$). The electric dipole moment operator transforms as A_1^-, giving $A_1^\pm \leftrightarrow A_1^\mp$, $A_2^\pm \leftrightarrow A_2^\mp$, $B_1^\pm \leftrightarrow B_1^\mp$, $B_2^\pm \leftrightarrow B_2^\mp$, and $E^\pm \leftrightarrow E^\mp$ selection rules on the rovibronic species.

The large number of vanishing states in N_2O_5 is a consequence of the spin-zero oxygen nuclei, which allow only rovibronic species which are symmetric with respect to interchange of the equivalent oxygen nuclei. In the case of $^{15}N_2O_5$ (which was not studied in the present investigation) the total wave function must be of B_1^+ or B_1^- symmetry. Again, the allowed rovibronic states have A_1^+, A_1^-, B_1^+, and B_1^- symmetry, however, for spin-1/2 ^{15}N the $A_1^\pm$ states have a statistical weight of 1 ($I_N=0$) and the $B_1^\pm$ states have a statistical weight of 3 ($I_N=1$). To increase the number of observed states while still having the molecular dynamics described by the G_{16} molecular symmetry group requires ^{17}O oxygen substitution ($I=5/2$) on all the oxygens of the NO_2 groups. The cost of such an experiment is prohibitive in our case.

The group theory allows us to construct a symmeterized basis set for discussing the dynamics of N_2O_5. Neglecting the small amplitude coordinates, an appropriate coordinate system for describing the rotation–internal rotation dynamics of N_2O_5 consists of the three Euler angles (θ,ϕ,χ)[36] relating the body-fixed and space-fixed Cartesian coordinate systems and the two internal-rotation angles, α_1 and α_2 (see Fig. 1). We fix the right-handed body-fixed axis system so that the y axis is normal to the N_a–O–N_b plane, the x axis bisects the N_a–O–N_b angle with the positive x direction pointing from the N's to the O, and the z axis is parallel to a line connecting N_b to N_a, with the positive z direction pointing from N_b to N_a.

In Table VII we show the transformation properties of the Euler and internal-rotation angles under the effects of the operations of the molecular-symmetry group. Also given are the equivalent rotations of Bunker[37] for each operation. From the transformation properties of the Euler angles, or similarly from the equivalent rotations, we can determine the symmetry properties of the rotational wave functions specifying the

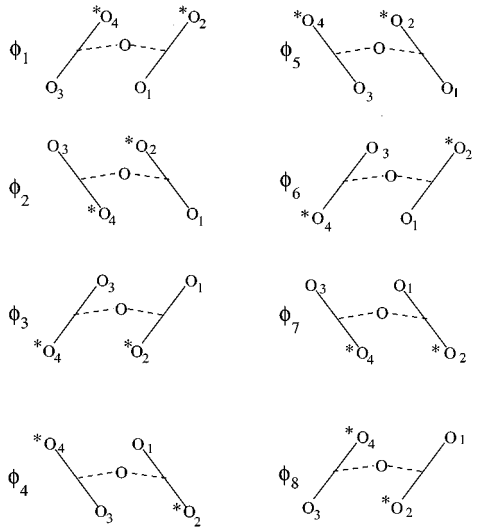

FIG. 7. The eight configurations responsible for the eightfold structural degeneracy of a nontunneling/noninternally rotating N_2O_5. The vibrational wave functions for the eight configurations are denoted ϕ_1 through ϕ_8. The even-numbered oxygen nuclei are labeled with asterisks for clarity.

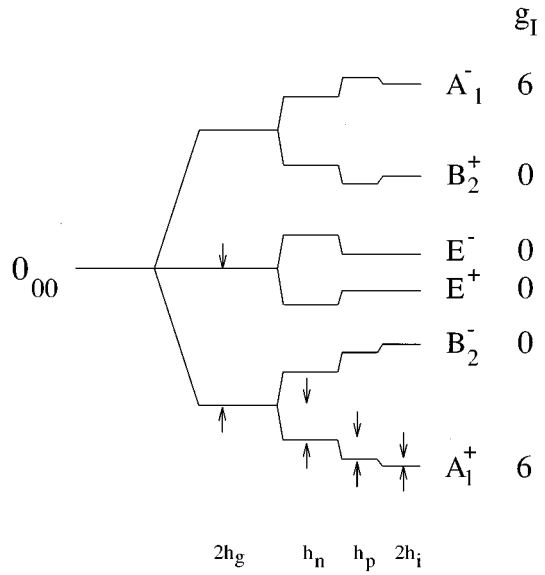

FIG. 9. Qualitative energy level diagram for $J=0$ N_2O_5 showing the lifting of the eightfold structural degeneracy of the rigid molecule through internal-rotation tunneling of the oxygen nuclei. The h's are tunneling matrix elements and are defined in the text.

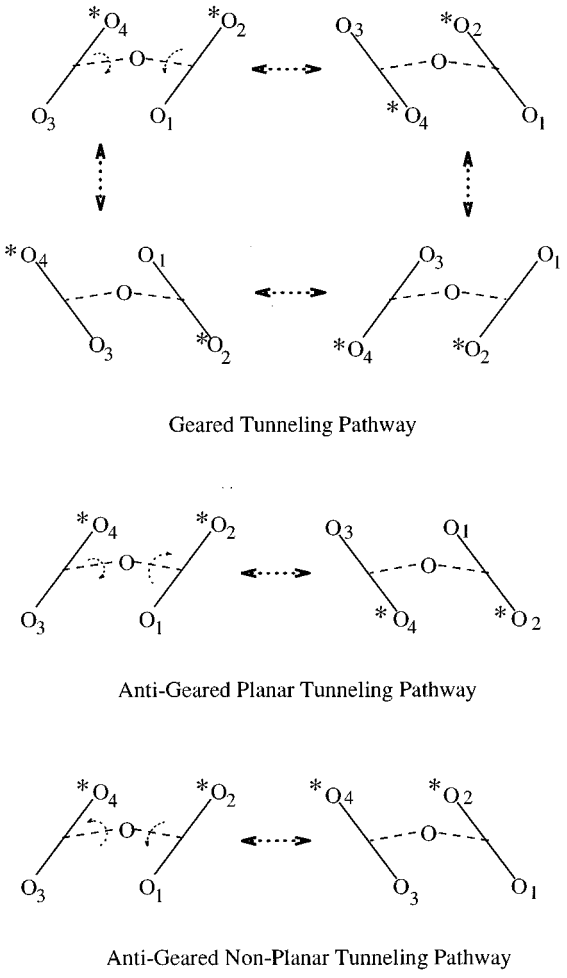

FIG. 8. Possible tunneling pathways for oxygen interchange in N_2O_5. The bridging O is furthest away from the reader. The even-numbered oxygen nuclei are labeled with an asterisks for clarity.

relative orientation of the (x,y,z) body-fixed axis system to the space-fixed axis system. For a I^r representation[11] the Wang symmetric-rotor functions[37] have the symmetries A_1^+, B_1^-, A_1^-, and B_1^+ for the $|K_aK_c\rangle=|ee\rangle$, $|eo\rangle$, $|oo\rangle$, and $|oe\rangle$ states, respectively, where e and o refer to the limiting K_a or K_c quantum number being even or odd. Similarly, using the transformation properties of the internal-rotation angles we can use projection operators to construct symmeterized internal-rotation wave functions from an unsymmeterized basis set consisting of products of $\sin(n\alpha_1)$ or $\cos(n\alpha_1)$ with $\sin(m\alpha_2)$ or $\cos(m\alpha_2)$ where n,m are integers. These symmeterized internal rotor functions are listed in Table VIII. Products of the symmeterized internal-rotor functions and the Wang symmetric rotor functions are used as basis func-

TABLE VII. Equivalent rotations and effects of symmetry operations on internal rotation and Euler angles for N_2O_5.

E	α_1	α_2	θ	ϕ	χ	R^0
(12)(34)	$\alpha_1+\pi$	$\alpha_2+\pi$	θ	ϕ	χ	R^0
(12)	$\alpha_1+\pi$	α_2	θ	ϕ	χ	R^0
(34)	α_1	$\alpha_2+\pi$	θ	ϕ	χ	R^0
(ab)(14)(23)	α_2	α_1	$\pi-\theta$	$\phi+\pi$	$2\pi-\chi$	R_x^π
(ab)(13)(24)	$\alpha_2+\pi$	$\alpha_1+\pi$	$\pi-\theta$	$\phi+\pi$	$2\pi-\chi$	R_x^π
(ab)(1423)	$\alpha_2+\pi$	α_1	$\pi-\theta$	$\phi+\pi$	$2\pi-\chi$	R_x^π
(ab)(1324)	α_2	$\alpha_1+\pi$	$\pi-\theta$	$\phi+\pi$	$2\pi-\chi$	R_x^π
E^*	$2\pi-\alpha_1$	$2\pi-\alpha_2$	$\pi-\theta$	$\phi+\pi$	$\pi-\chi$	R_y^π
(12)(34)*	$\pi-\alpha_1$	$\pi-\alpha_2$	$\pi-\theta$	$\phi+\pi$	$\pi-\chi$	R_y^π
(12)*	$\pi-\alpha_1$	$2\pi-\alpha_2$	$\pi-\theta$	$\phi+\pi$	$\pi-\chi$	R_y^π
(34)*	$2\pi-\alpha_1$	$\pi-\alpha_2$	$\pi-\theta$	$\phi+\pi$	$\pi-\chi$	R_y^π
(ab)(14)(23)*	$2\pi-\alpha_2$	$2\pi-\alpha_1$	θ	ϕ	$\chi+\pi$	R_z^π
(ab)(13)(24)*	$\pi-\alpha_2$	$\pi-\alpha_1$	θ	ϕ	$\chi+\pi$	R_z^π
(ab)(1324)*	$2\pi-\alpha_2$	$\pi-\alpha_1$	θ	ϕ	$\chi+\pi$	R_z^π
(ab)(1423)*	$\pi-\alpha_2$	$2\pi-\alpha_1$	θ	ϕ	$\chi+\pi$	R_z^π

TABLE VIII. Symmetrized internal-rotor basis functions for N_2O_5.[a,b]

A_1^+	$\cos(n\alpha_1)\cos(m\alpha_2)+\cos(n\alpha_2)\cos(m\alpha_1)$	$n\geqslant m\geqslant 0$	n even, m even
	$\sin(n\alpha_1)\sin(m\alpha_2)+\sin(n\alpha_2)\sin(m\alpha_1)$	$n\geqslant m\geqslant 2$	n even, m even
A_1^-	$\sin(n\alpha_1)\cos(m\alpha_2)+\sin(n\alpha_2)\cos(m\alpha_1)$	$n>m\geqslant 0$	n even, m even
	$\cos(n\alpha_1)\sin(m\alpha_2)+\cos(n\alpha_2)\sin(m\alpha_1)$	$n\geqslant m\geqslant 2$	n even, m even
B_1^+	$\cos(n\alpha_1)\cos(m\alpha_2)-\cos(n\alpha_2)\cos(m\alpha_1)$	$n>m\geqslant 0$	n even, m even
	$\sin(n\alpha_1)\sin(m\alpha_2)-\sin(n\alpha_2)\sin(m\alpha_1)$	$n>m\geqslant 2$	n even, m even
B_1^-	$\sin(n\alpha_1)\cos(m\alpha_2)-\sin(n\alpha_2)\cos(m\alpha_1)$	$n>m\geqslant 0$	n even, m even
	$\cos(n\alpha_1)\sin(m\alpha_2)-\cos(n\alpha_2)\sin(m\alpha_1)$	$n\geqslant m\geqslant 2$	n even, m even
A_2^+	$\cos(n\alpha_1)\cos(m\alpha_2)-\cos(n\alpha_2)\cos(m\alpha_1)$	$n>m\geqslant 1$	n odd, m odd
	$\sin(n\alpha_1)\sin(m\alpha_2)-\sin(n\alpha_2)\sin(m\alpha_1)$	$n>m\geqslant 1$	n odd, m odd
A_2^-	$\sin(n\alpha_1)\cos(m\alpha_2)-\sin(n\alpha_2)\cos(m\alpha_1)$	$n>m\geqslant 1$	n odd, m odd
	$\cos(n\alpha_1)\sin(m\alpha_2)-\cos(n\alpha_2)\sin(m\alpha_1)$	$n\geqslant m\geqslant 1$	n odd, m odd
B_2^+	$\cos(n\alpha_1)\cos(m\alpha_2)+\cos(n\alpha_2)\cos(m\alpha_1)$	$n\geqslant m\geqslant 1$	n odd, m odd
	$\sin(n\alpha_1)\sin(m\alpha_2)+\sin(n\alpha_2)\sin(m\alpha_1)$	$n\geqslant m\geqslant 1$	n odd, m odd
B_2^-	$\sin(n\alpha_1)\cos(m\alpha_2)+\sin(n\alpha_2)\cos(m\alpha_1)$	$n>m\geqslant 1$	n odd, m odd
	$\cos(n\alpha_1)\sin(m\alpha_2)+\cos(n\alpha_2)\sin(m\alpha_1)$	$n\geqslant m\geqslant 1$	n odd, m odd
E_1^+	$\cos(n\alpha_1)\cos(m\alpha_2)+\cos(n\alpha_2)\cos(m\alpha_1)$	$n\geqslant 1, m\geqslant 0$	n odd, m even
	$\sin(n\alpha_1)\sin(m\alpha_2)+\sin(n\alpha_2)\sin(m\alpha_1)$	$n\geqslant 1, m\geqslant 2$	n odd, m even
E_2^+	$\cos(n\alpha_1)\cos(m\alpha_2)-\cos(n\alpha_2)\cos(m\alpha_1)$	$n\geqslant 1, m\geqslant 0$	n odd, m even
	$\sin(n\alpha_1)\sin(m\alpha_2)-\sin(n\alpha_2)\sin(m\alpha_1)$	$n\geqslant 1, m\geqslant 2$	n odd, m even
E_1^-	$\sin(n\alpha_1)\cos(m\alpha_2)+\sin(n\alpha_2)\cos(m\alpha_1)$	$n\geqslant 1, m\geqslant 0$	n odd, m even
	$\cos(n\alpha_1)\sin(m\alpha_2)+\cos(n\alpha_2)\sin(m\alpha_1)$	$n\geqslant 1, m\geqslant 2$	n odd, m even
E_2^-	$\sin(n\alpha_1)\cos(m\alpha_2)-\sin(n\alpha_2)\cos(m\alpha_1)$	$n\geqslant 1, m\geqslant 0$	n odd, m even
	$\cos(n\alpha_1)\sin(m\alpha_2)-\cos(n\alpha_2)\sin(m\alpha_1)$	$n\geqslant 1, m\geqslant 2$	n odd, m even

[a]Functions are not normalized.
[b]The subscripts on the E species are not symmetry labels but refer to the two sets of functions which make up the degenerate E species.

tions for diagonalizing the rotation–internal rotation Hamiltonian of N_2O_5.

To construct the Hamiltonian operator for N_2O_5 we first express the space-fixed Cartesian coordinates of each atom in terms of $(\theta,\phi,\chi,\alpha_1,\alpha_2)$ and the fixed bond angles and bond lengths (R,r,γ,β) to obtain a kinetic energy expression in terms of the Euler and internal-rotation angles and their velocities. After ignoring terms associated with translation of the center of mass we obtain the following expression for the classical kinetic energy:

$$\begin{aligned}2T=&I_{xx}\omega_x^2+I_{yy}\omega_y^2+I_{zz}\omega_z^2+2I_{xy}\omega_x\omega_y+2I_{xz}\omega_x\omega_z\\&+2I_{yz}\omega_y\omega_z+I_0(\dot\alpha_-^2+\dot\alpha_+^2)+\sqrt{2}I_0\lambda_z\omega_z\dot\alpha_-\\&-\sqrt{2}I_0\lambda_x\omega_x\dot\alpha_+,\end{aligned}\tag{5}$$

where I_{ij} $(i,j=x,y,z)$ are the components of the total inertial tensor of the molecule and are functions of α_1 and α_2, ω_i $(i=x,y,z)$ are the angular velocities about the i'th axis, I_0 is the moment of inertia of an NO_2 group about its C_2 axes, $\lambda_x=\cos(\gamma/2)$ and $\lambda_z=\sin(\gamma/2)$ are the direction cosines between the NO_2 top C_2 axes and the x and z axes, respectively, $\dot\alpha_+=(\dot\alpha_1+\dot\alpha_2)/\sqrt{2}$ and $\dot\alpha_-=(\dot\alpha_1-\dot\alpha_2)/\sqrt{2}$. Because of our choice of the inertial frame, $\dot\alpha_+$ couples only with ω_x and $\dot\alpha_-$ couples only with ω_z.

In the spirit of Hougen, Bunker, Johns[36] and others, Eq. (5) can be rewritten as

$$2T=\omega^+\mathbf{I}\omega,\tag{6}$$

where $\mathbf{I}$ is a 5 dimensional generalized inertia tensor and $\boldsymbol{\omega}^+=(\omega_x,\omega_y,\omega_z,\dot\alpha_+,\dot\alpha_-)$ is a row vector and $\boldsymbol{\omega}$ is its transpose. Expressing T in terms of momenta we have

$$2T=\mathbf{p}^+\boldsymbol{\mu}\mathbf{p},\tag{7}$$

where the elements of $\mathbf{p}^+=(P_x,P_y,P_z,P_+,P_-)$ are the generalized momenta associated with the angular velocities of $\boldsymbol{\omega}^+$, and $\boldsymbol{\mu}$ is the inverse inertia tensor, the elements of which are functions of α_1 and α_2.

Using standard procedures[37,38] for converting the classical Hamiltonian to the quantum mechanical operator we obtain the following rotation–internal-rotation Hamiltonian for N_2O_5:

$$H=\sum\ \tfrac{1}{2}P_i\mu_{ij}P_j+V_{\rm eff}(\alpha_1,\alpha_2)+V(\alpha_1,\alpha_2),\tag{8}$$

where the summation runs over the five momenta, $V_{\rm eff}$ is a small effective potential arising from the transformation of the kinetic-energy operator to quantum mechanical form,[39] and V is the internal-rotation potential. Since $V_{\rm eff}$ is expected to be negligible compared to V we will ignore its contributions to H in the present discussion. The symmetries of the various operators of H are summarized in Table IX.

The Hamiltonian matrix of H is set up in the symmeterized rotation–internal-rotation basis. The evaluation of the matrix elements containing the μ_{ij} components or V is simplified by expanding each of these operators in the basis functions of the correct symmetry. In our initial calculation of the rotation–tunneling levels we follow McClelland *et al.*[7] and choose a trial potential of the form

TABLE IX. Symmetries of various operators in G_{16}.

Angular momentum operators					
	P_x	P_y	P_z	P_+	P_-
	A_1^-	B_1^+	B_1^-	A_1^-	B_1^-
μ_{ij} matrix elements					
$i\backslash j$	x	y	z	$+$	$-$
x	A_1^+	B_1^-	B_1^+	A_1^+	B_1^+
y		A_1^+	A_1^-	B_1^-	A_1^-
z			A_1^+	B_1^+	A_1^+
$+$				A_1^+	B_1^+
$-$					A_1^+

$$V(\alpha_1\alpha_2)=\frac{V_0}{2}(2-\cos 2\alpha_1-\cos 2\alpha_2)+U_0\sum (r_0/r_{ij})^n, \tag{9}$$

where the first term allows for electronic contributions to the potential due to coupling of the two NO_2 groups through the NON frame and the second term mimics the van der Waals repulsions of the O atoms between the two NO_2 groups, with r_{ij} being the separation of the ith and jth O nuclei of the two NO_2 units. The electron-diffraction potential of McClelland *et al.*[7] has $V_0=665(84)$ cm^{-1}, $U_0=35$ cm^{-1}, $r_0=2.8$ Å, and $n=12$.

Initial dynamical calculations were undertaken on the electron-diffraction potential to compare predictions from this surface with the experimental results. Because of the anisotropy of this potential, the basis-set expansion requires internal rotor states with n and m as large as 24 for the basis functions shown in Table VIII, leading to diagonalization of matrices as large as 481×481 for $J=1$. The results from the calculations show that the electron-diffraction potential is much too anisotropic and favors a tunneling pathway which is inconsistent with experiment. The predicted tunneling splittings for the A_1^- and A_1^+ are less than 100 kHz and essentially identical rotational constants are calculated for the two states ($A=7019$ MHz, $B=2032$ MHz, $C=1779$ MHz). The zero-statistical-weight, $J=0$, B_2^+ and B_2^- states are also degenerate with each other, as are the zero-weight, E^+ and E^- states. The B_2^+ and B_2^- pair are separated from the A_1^+ and A_1^- pair by 8 MHz, with the E^+ and E^- states falling in between. Experimentally, we observe that the A_1^- and A_1^+ transitions are split in some cases by more than 2 GHz, suggesting that the tunneling splittings are more on the order of GHz than kHz. The dominant electron-diffraction tunneling pathway, splits the $A_1^\pm$ and $B_2^\pm$ species symmetrically from the $E^\pm$ species, and mimics the independent internal rotation of one of the two NO_2 groups by 180° about its C_2 axis, corresponding to the tunneling matrix element h_i of Eqs. (3) and (4).

We have attempted to vary the potential parameters of the electron-diffraction potential to obtain results which are more consistent with experiment. This process turns out to be difficult because the spectroscopic data is only weakly sensitive to the potential barrier heights due to the lack of any direct measure of the $J=0$ tunneling splitting and because the vanishing statistical weights for many of the states prevents their observation. Alternatively, we have used the *ab initio* calculations to model the general features of the tunneling potential for N_2O_5. The *ab initio* calculations indicate that the configurations where $\alpha_1=\alpha_2=0$ and $\alpha_1=\alpha_2=90°$ correspond to high energy maxima on the internal-rotation potential. The lowest energy extrema on the potential energy surface correspond to $\alpha_1=0$ and $\alpha_2=90°$ or $\alpha_1=90°$ and $\alpha_2=0$ and the C_2 configuration observed experimentally. The *ab initio* calculations suggest that the most reasonable tunneling motion for interchanging the bonding roles of the two NO_2 groups is the geared pathway of Fig. 8. A two dimensional potential energy surface which qualitatively represents these features is given by

$$V(\alpha_1,\alpha_2)=-V_{\text{geared}}\cos[2(\alpha_2-\alpha_1)]+V_{\text{antigeared}}e^{\delta[1-\sin^2(\alpha_2+\alpha_1)]}+V_{\text{linear}}(\cos 2\alpha_1+\cos 2\alpha_2), \tag{10}$$

where the V_{geared} term characterizes the barrier at $\alpha_1=0$ and $\alpha_2=90°$ (or $\alpha_1=90°$ and $\alpha_2=0$), the $V_{\text{antigeared}}$ term forces the NO_2 groups to move preferentially in a geared motion, and V_{linear} is necessary to allow the potential minimum to move away from an $\alpha_1=\alpha_2=45°$ configuration.

The qualitative features of the spectrum are only reproduced by having very small barriers ($<\sim10$ cm^{-1}) hindering the geared internal rotation of the two NO_2 groups. For example, if we use values of V_{geared}, $V_{\text{antigeared}}$, δ, and V_{linear} of 0, 120 cm^{-1}, 2, and -40 cm^{-1}, which gives a barrier of ~7 cm^{-1} to geared internal rotation, we calculate large splittings of the transitions (2.0 GHz for the two $1_{11}-0_{00}$ lines, 1.3 GHz for the $2_{20}-1_{11}$ lines, and 3.7 GHz for the $2_{21}-1_{10}$ lines) for the two tunneling states, of the same order of magnitude as the experimental observations. In addition, this potential has a minimum at $\alpha_1=\alpha_2=41°$, as expected from the quadrupole hyperfine analysis, and no other low lying tunneling states are predicted to be observable experimentally, in agreement with the detection of only one pair of tunneling states.

IV. DISCUSSION

The microwave spectrum of N_2O_5 is consistent with the earlier electron-diffraction results[7] which determined a C_2 symmetry structure for the molecule. The present microwave and *ab initio* calculations further demonstrate that N_2O_5 has a large-amplitude motion corresponding to the geared rotation of the two NO_2 groups about their twofold axes. The lack of any direct measurement of the tunneling splitting associated with this motion makes it difficult to precisely determine the barrier, however, our model simulations suggest that the barrier is on the order of 10 cm^{-1}, significantly smaller than the electron-diffraction value of ~200 cm^{-1}.[7] A possible source of error in the electron-diffraction analysis may be due to the lack of correction for background nitric acid impurity, which was found to be a dominant impurity in the present experiments.

The small magnitude of the barrier in N_2O_5 makes it essential to understand the large-amplitude potential and its effect on the rotational and vibrational states of the molecule to accurately model the thermodynamic properties of N_2O_5 in atmospheric chemistry applications. For molecules where the internal rotor is a symmetric top, precise internal-rotation barriers have been determined without direct measurement of the tunneling splitting. However, for such molecules there is no dependence of the overall rotational constants on the internal rotation angles, making it easier to model the Coriolis contributions to the rotational constants from which the barrier is inferred. In the case of N_2O_5, the rotational constants vary greatly with internal rotation angles due to the large masses of the oxygen nuclei. Because of the significant dependence of the rotational constants on the internal-rotation angles, more general internal-axis models (IAM) such as applied by Coudert and Hougen[40] to $(H_2O)_2$ would need to include the internal-rotation dependence of the rotational constants explicitly.

Additional information on the structure and tunneling pathways in N_2O_5 can be obtained by isotopic substitution. For instance, mono ^{17}O or ^{18}O substitution on one of the NO_2 groups removes the antigeared nonplanar tunneling pathway. The geared pathway is also affected since now all four minima are no longer isoenergetic. Mono ^{15}N substitution does not affect the qualitative features of any of the tunneling motions shown in Fig. 8. We note that in most cases isotopic substitution will significantly change the simplicity of the spectrum arising from the Boson statistics of the four equivalent spin-zero oxygens of the NO_2 groups.

The structure inferred from the electron-diffraction experiment[7] is somewhat more planar than that inferred from the present work. The diffraction experiment led to a value of $\alpha \approx 30°$, whereas the present experiments indicate $\alpha \approx 41°$ and the *ab initio* calculations yield $\alpha = 37°$. The spread among these values reflects the flatness of the torsional potential, as described above. For bond lengths and angles, the MP2 and QCISD values generally agree better with experiment than do the density-functional values from the present work and from Ref. 9. Density-functional theory appears to have some trouble describing the bonding at the central oxygen atom; the bond length R and bond angle γ are too large compared with experiment.

The vibrational frequencies of Table V compare reasonably well with those from density-functional calculations and from experiment.[9,41] However, the density-functional results agree better with experiment and therefore appear more reliable. All the theoretical vibrational frequencies indicate that the experimental assumption of multiple degeneracies[41] is incorrect. Failure to resolve peaks is probably due to intensity differences instead of accidental degeneracies.

The largest discrepancy between theory and experiment is for the dipole moment. The computed QCISD value is $\mu = 0.24$ D, and values from 0.14 to 0.31 D were obtained in a density-functional study.[9] Consistent with theory, the intensities in the present experiment suggest $\mu \sim 0.5$ D. A value of 1.39 D, however, was inferred from measurements in CCl_4 solution.[10] There are two simple alternative explanations for the discrepancy with the solution measurement. The sample may have been contaminated with HNO_3, the product of the facile hydrolysis of N_2O_5. Since $\mu(HNO_3) = 2.17 \pm 0.02$ D,[42] such contamination would lead to a high measured value. Alternatively, N_2O_5 may adopt a different conformation in solution than in the gas phase. Only a small differential solvation energy ($\lesssim 2$ kJ/mol) is required to favor structure **2** over **1**. Since conformation **2** is predicted to have a larger dipole moment than structure **1** (Table III), solvation effects may explain the high solution value for μ.

ACKNOWLEDGMENTS

The authors would like to thank the Upper-Atmosphere Research Program of NASA and NATO (Grant No. CRG931359) for partial support of this work. J.-U.G. acknowledges postdoctoral fellowship support from the Deutsche Forschungsgemeinschaft.

[1] G. C. Toon, C. B. Farmer, and R. H. Norton, Nature (London) **319**, 570 (1986).
[2] C. Camy-Peyret, J.-M. Flaud, L. Lechuga-Fossat, G. Laverdet, and G. Le Bras, Chem. Phys. Lett. **139**, 345 (1987).
[3] C. A. Cantrell, J. A. Davidson, A. H. McDaniel, R. E. Shetter, and J. G. Calvert, Chem. Phys. Lett. **148**, 358 (1988).
[4] F. C. De Lucia, B. P. Winnewisser, M. Winnewisser, and G. Pawelke, J. Mol. Spectrosc. **136**, 151 (1989).
[5] J.-M. Colmont, J. Mol. Spectrosc. **155**, 11 (1992).
[6] D. Newnham, J. Ballard, and M. Page, J. Quant. Spectrosc. Radiat. Transfer **50**, 571 (1993).
[7] B. W. McClelland, L. Hedberg, K. Hedberg, and K. Hagen, J. Am. Chem. Soc. **105**, 3789 (1983).
[8] J. E. Carpenter and G. M. Maggiora, Chem. Phys. Lett. **87**, 349 (1982).
[9] A. Stirling, I. Pápai, J. Mink, and D. R. Salahub, J. Chem. Phys. **100**, 2910 (1994).
[10] G. L. Lewis and C. P. Smyth, J. Am. Chem. Soc. **61**, 3067 (1939).
[11] J. K. G. Watson, in *Vibrational Spectra and Structure*, edited by J. R. Durig, (Elsevier, Amsterdam, 1978), Vol. 6, pp. 1–89.
[12] G. V. Caesar and M. Goldfrank, J. Am. Chem. Soc. **68**, 372 (1946).
[13] P. W. Schenk, in *Handbook of Preparative Inorganic Chemistry*, edited by G. Brauer (Academic, New York, 1963), Vol. 1, pp. 489–491.
[14] T. J. Balle and W. H. Flygare, Rev. Sci. Instrum. **52**, 33 (1981).
[15] F. J. Lovas and R. D. Suenram, J. Chem. Phys. **87**, 2010 (1987); R. D. Suenram, F. J. Lovas, G. T. Fraser, J. Z. Gillies, C. W. Gillies, and M. Onda, J. Mol. Spectrosc. **137**, 127 (1989); F. J. Lovas, N. Zobov, G. T. Fraser, and R. D. Suenram, J. Mol. Spectrosc. **171**, 189 (1995).
[16] J.-U. Grabow and W. Stahl, Z. Naturforsch. Teil A **45**, 1043 (1990).
[17] J. Z. Gillies, C. W. Gillies, F. J. Lovas, K. Matsumura, R. D. Suenram, E. Kraka, and D. Cremer, J. Am. Chem. Soc. **113**, 6408 (1991).
[18] U. Andresen, H. Dreizler, J.-U. Grabow, and W. Stahl, Rev. Sci. Instrum. **61**, 3694 (1990).
[19] J. C. Slater, *The Self-Consistent Field for Molecules and Solids, Vol. 4: Quantum Theory of Molecules and Solids* (McGraw-Hill, New York, 1974).
[20] S. H. Vosko, L. Wilk, and M. Nusair, Can. J. Phys. **58**, 1200 (1980).
[21] A. D. Becke, Phys. Rev. A **38**, 3098 (1988).
[22] C. Lee, W. Yang, and R. G. Parr, Phys. Rev. B **37**, 785 (1988).
[23] P. J. Stephens, F. J. Devlin, C. F. Chabalowski, and M. J. Frisch, J. Phys. Chem. **98**, 11623 (1994).
[24] A. D. Becke, J. Chem. Phys. **98**, 5648 (1993).
[25] L. Albinus, J. Spieckermann, and D. H. Sutter, J. Mol. Spectrosc. **133**, 128 (1989).
[26] M. H. Palmer, J. Mol. Struct. **239**, 173 (1990).
[27] M. J. Frisch, G. W. Trucks, H. B. Schlegel, P. M. W. Gill, B. G. Johnson, M. W. Wong, J. B. Foresman, M. A. Robb, M. Head-Gordon, E. S. Replogle, R. Gomperts, J. L. Andres, K. Raghavachari, J. S. Binkley, C. Gonzalez, R. L. Martin, D. J. Fox, D. J. Defrees, J. Baker, J. J. P. Stewart, and J. A. Pople, GAUSSIAN 92/DFT, Gaussian, Inc., Pittsburgh, PA, 1993.

[28] M. J. Frisch, G. W. Trucks, H. B. Schlegel, P. M. W. Gill, B. G. Johnson, M. A. Robb, J. R. Cheeseman, T. Keith, G. A. Peterson, J. A. Montgomery, K. Raghavachari, M. A. Al-Laham, V. G. Zakrzewski, J. V. Ortiz, J. B. Foresman, J. Cioslowski, B. B. Stefanov, A. Nanayakkara, M. Challacombe, C. Y. Peng, P. Y. Ayala, W. Chen, M. W. Wong, J. L. Andres, E. S. Replogle, R. Gomperts, R. L. Martin, D. J. Fox, J. S. Binkley, D. J. Defrees, J. Baker, J. P. Stewart, M. Head-Gordon, C. Gonzalez, and J. A. Pople, GAUSSIAN 94, Revision A.1, Gaussian, Inc., Pittsburgh, PA, 1995.

[29] ACES II, an ab initio program system authored by J. F. Stanton, J. Gauss, J. D. Watts, W. J. Lauderdale, and R. J. Bartlett. The package also contains modified versions of the MOLECULE Gaussian integral program of J. Almlöf and P. R. Taylor, the ABACUS integral derivative program of T. U. Helgaker, H. J. A. Jense, P. Jorgensen, and P. R. Taylor, and the PROPS property integral package of P. R. Taylor.

[30] J. F. Stanton, J. Gauss, J. D. Watts, W. J. Lauderdale, and R. J. Bartlett, Int. J. Quantum Chem. S **26**, 879 (1992).

[31] Certain commercial materials and equipment are identified in this paper in order to specify procedures completely. In no case does such identification imply recommendation or endorsement by the National Institute of Standards and Technology, nor does it imply that the material or equipment identified is necessarily the best available for the purpose.

[32] See AIP document No. PAPS JCPSA-105-7249-3 for 3 pages of measured microwave transition frequencies for N_2O_5. Order by PAPS number and journal reference from American Institute of Physics, Physics Auxiliary Publication Service, Carolyn Gehlbach, 500 Sunnyside Boulevard, Woodbury, New York 11797-2999. Fax: 516-576-2223, e-mail: paps@aip.org. The price is $1.50 for each microfiche (98 pages) or $5.00 for photocopies of up to 30 pages, and $0.15 for each additional page over 30 pages. Airmail additional. Make checks payable to the American Institute of Physics.

[33] C. H. Townes and A. L. Schalow, *Microwave Spectroscopy* (Dover, New York, 1975), pp. 149–173.

[34] H. C. Longuet-Higgins, Mol. Phys. **6**, 445 (1963).

[35] D. R. Dyke, J. Chem. Phys. **66**, 492 (1977).

[36] J. T. Hougen, P. R. Bunker, and J. W. C. Johns, J. Mol. Spectrosc. **34**, 136 (1970).

[37] E. Bright Wilson, Jr., J. C. Decius, and P. C. Cross, *Molecular Vibrations* (Dover, New York, 1955).

[38] P. R. Bunker, *Molecular Symmetry and Spectroscopy* (Academic, New York, 1979).

[39] V_{eff} has the form $V_{\text{eff}}=\Sigma_{ij}[(-5/32g^2)\mu_{ij}(P_ig)(P_jg)+(1/8g)(P_i\mu_{ij})(P_jg)+(1/8g)\mu_{ij}[P_i(P_jg)]]$, where the i and j summation is over the two tops $(i,j=4,5)$, g is a determinant of the $\boldsymbol{\mu}$ inverse tensor matrix, and the P_i operations are confined to be within the first surrounding parenthesis or brackets.

[40] L. H. Coudert and J. T. Hougen, J. Mol. Spectrosc. **130**, 86 (1988).

[41] I. C. Hisatune, J. P. Devlin, and Y. Wada, Spectrochim. Acta. **18**, 1641 (1962).

[42] A. P. Cox and J. M. Riveros, J. Chem. Phys. **42**, 3106 (1965).